

Coupled channel folding model description of α scattering from ${}^9\text{Be}$

Subinit Roy, J. M. Chatterjee, and H. Majumdar
Saha Institute of Nuclear Physics, 1/AF Bidhannagar, Calcutta 700064, India

S. K. Datta
Nuclear Science Centre, P.O.10502, New Delhi 110067, India

S. R. Banerjee
Variable Energy Cyclotron Centre, 1/AF Bidhannagar, Calcutta 700064, India

S. N. Chintalapudi
Inter-University Consortium, Department of Atomic Energy Facilities, Bidhannagar, Calcutta 700064, India
 (Received 5 July 1994; revised manuscript received 19 April 1995)

Alpha scattering from ${}^9\text{Be}$ at $E_\alpha = 65$ MeV is described in the coupled channel framework with phenomenological as well as folded potentials. The multipole components of the deformed density of ${}^9\text{Be}$ are derived from Nilsson model wave functions. Reasonably good agreements are obtained for the angular distributions of $3/2^-$ (g.s.) and $5/2^-$ (2.43 MeV) states of the ground state band with folded potentials. The deformation predicted by the model corroborates with that derived from the phenomenological analysis with potentials of different geometries.

PACS number(s): 25.55.Ci, 21.10.Ky, 24.10.Eg, 27.20.+n

I. INTRODUCTION

Among the p -shell nuclei ${}^9\text{Be}$ with its location near the middle of the shell is expected to have a large deformation [1]. Several investigations of the structure of this extremely deformed nucleus have been made with different probes like electron scattering [2–4], pion scattering [5], and proton and alpha scattering [6–12]. The estimate of the equilibrium quadrupole deformation of ${}^9\text{Be}$ from these studies ranges from 0.52 to 1.3. Notwithstanding the different isospin selectivity of these probes and the large relative difference in the number of neutrons and protons in the p shell of ${}^9\text{Be}$, the spectrum of values of quadrupole deformation of the nucleus is uncomfortably broad.

We attempted to probe this aspect with inelastic scattering of α particles from ${}^9\text{Be}$. The angular distribution of inelastic scattering of “isoscalar” α particles gives a measure of the mass deformation of the target nucleus. The deformation required to generate the effective transition potentials, the off-diagonal component of the α -nucleus potential matrix describing the scattering, is actually related to the deformation of the target nucleus. For deformed ${}^9\text{Be}$ with ground state spin $3/2$, the optical potential is itself a deformed one. The diagonal terms of the matrix representing such a potential are responsible for the elastic scattering and other self-coupling or “reorientation” effects. The previous two studies of α scattering from ${}^9\text{Be}$, in the framework of a strong coupling approximation, predicted the quadrupole deformation parameter as 0.52 [11] and 0.9 [12], respectively. However, the resulting optical potentials have distinctly different geometrical parameters. In this context, we present a study of inelastic scattering of 65 MeV α particles from rotational states of the ground state band ($K=3/2^-$) of ${}^9\text{Be}$ with a phenomenological as well as semimicroscopic folding model potential.

We assumed ${}^9\text{Be}$ to be a symmetric rotor and performed

an explicit coupled channel (CC) calculation with the members of the ground state band only. Unlike as in Ref. [12], where a “fictitious” $0^+ \rightarrow 2^+$ system was constructed from the data of $3/2^-$ and $5/2^-$ states for the analysis to take into account the quadrupole scattering effect in the elastic angular distribution, we worked with proper spins of the states. Considering quadrupole coupling between the states and reorientation coupling of same multipolarity for each state we found that the quadrupole scattering effect automatically gets included and the model is a better representation of ${}^9\text{Be}$. The quadrupole deformation obtained in the phenomenological description with this coupling scheme shows a distinct preference for lower values even with largely different geometrical parameters of the phenomenological Woods-Saxon potentials. On the other hand, in the folding model approach the interaction potential is generated by folding the density-dependent M3Y interaction with the deformed density distribution of ${}^9\text{Be}$. Thus the radial falloff of the potential is fixed by the range of the effective n - n interaction and the radial extent of the target projectile densities. The deformation of the target nucleus enters into the description through its density. We calculated the monopole and quadrupole components of the density from the Nilsson model wave functions. That the deformation can be used as an adjustable parameter in this model and the success of the model in describing the electron scattering form factors [2,3] prompted us to use the model in the analysis of the α scattering data also. We compared the resulting densities with those obtained from electron and proton scattering predictions. The deformation used in the folding model calculation is discussed in relation to that obtained from the phenomenological calculation.

The folding model analysis is performed also from an altogether different standpoint. In the description of α scattering from various nuclei, the model was found to be quite successful [13,14]. It also gave a good account of the scat-

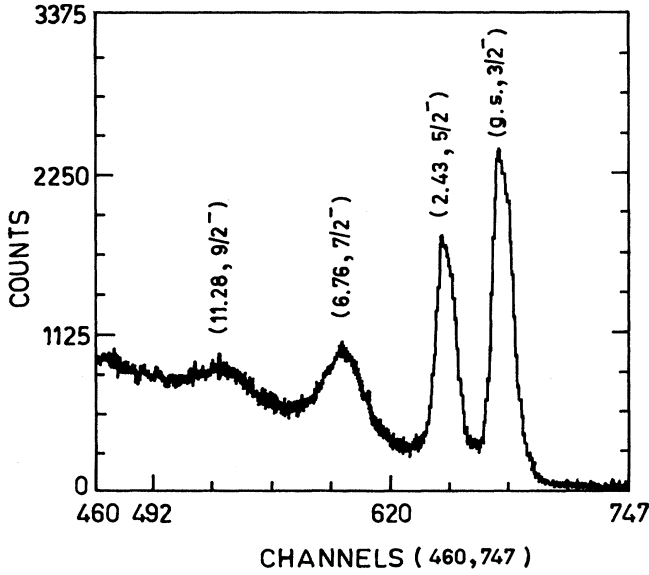


FIG. 1. The spectrum of 65 MeV α scattering from ${}^9\text{Be}$ at $\theta_{\text{lab}} = 42^\circ$.

tering of heavier projectiles [15,16]. But for the scattering of loosely bound light nuclei like ${}^6\text{Li}$ and ${}^9\text{Be}$ from heavier targets, the model overestimated the interaction potential by a large amount of 40–50% [15,16]. Again, recent studies of ${}^3,4\text{He}$ scattering from ${}^6\text{Li}$ [17] showed that consistently good agreement with the data of a large range of incident energies can be obtained with the values of the renormalization factor close to unity. Like ${}^6\text{Li}$, the breakup threshold (1.67 MeV) of ${}^9\text{Be}$ also lies just above the ground state. It will be of interest to see the outcome of the application of the model to describe the α scattering from ${}^9\text{Be}$.

II. EXPERIMENT

The experiment was performed with an unanalyzed beam from the Variable Energy Cyclotron Centre (VECC), Calcutta. The beam energy was 65.0 MeV. The self-supported ${}^9\text{Be}$ target was prepared at the VECC target laboratory from a 99% pure thin foil of beryllium. The target thickness was 1.85 mg/cm². Energy loss in the target for 65 MeV α particle is approximately 186 keV. The average beam current during the experiment was maintained at 60 nA. Two Si(Li) detectors of active thickness 2 mm each were used. The detectors were mounted at distances 28.332 cm and 25.792 cm with effective solid angles of 0.243 sr and 0.293 sr, respectively. Particle identifiers were not set up as the other competing channels like (α, p) , (α, d) , (α, t) , and $(\alpha, {}^3\text{He})$ have high negative Q values. The overall energy resolution of the detectors was tested with the ${}^{12}\text{C}$ target. With beam resolution being nearly 200 keV the energy resolutions were found to be 290 keV (D1) and 400 keV (D2), respectively. Data were collected from $\theta_{\text{lab}} = 20^\circ$ to $\theta_{\text{lab}} = 108^\circ$ in steps of 2° . A typical spectrum at $\theta_{\text{lab}} = 42^\circ$ is shown in Fig. 1. The error in the data is in the range of 20–25%. To have data for a wider angular range, the forward angle data from Ref. [11] were used and normalized to our data at $\theta_{\text{c.m.}} = 28.84^\circ$. The nor-

malization was found to differ by less than 8% from unity and it is well within the range of error in the data.

III. ANALYSIS

The spectrum of ${}^9\text{Be}$ exhibits simple rotational picture [18] with strongest excitations belonging to the ground state band of $K=3/2^-$. The ground state being a $3/2^-$ state, the other members of the band are identified as $5/2^-$ at 2.43 MeV and $7/2^-$ at 6.76 MeV [18]. (Recently it has been shown by Glickman *et al.* [4] and Dixit *et al.* [9] that the $7/2^-$ state of the band lies at 6.38 MeV with a new state of spin $9/2^+$ at 6.76 MeV. However, we still worked with the energy assignment of 6.76 MeV to the $7/2^-$ state according to Ref. [18] in our calculation.) The strong coupling model for ${}^9\text{Be}$ has been tested for electron scattering [2] and other hadronic probes [6,11,12,19,20] and found to improve the scattering predictions. The shell model [4,21] and cluster model [22] also predict a simple rotational picture for ${}^9\text{Be}$. In our coupled channel analysis we followed a scheme where the first three negative parity states of the ground state band were coupled explicitly. As the quadrupole moment of ${}^9\text{Be}$ is large the “reorientation” contributions, which are proportional to the quadrupole moment, were included in the coupling scheme. In the CC description, the reorientation term takes into account the effect of quadrupole scattering on the elastic angular distribution. Only the $L=2$ reorientation contributions were considered. The corresponding radial form factors were assumed to have the same shape as the $3/2^- - 5/2^-$ $L=2$ transition potential. However, the magnitudes were fixed from the corresponding nuclear reduced matrix elements. Coulomb excitation was also included in the calculation. Coupling to the higher excited band ($K=1/2^-$) with $1/2^-$ bandhead at 2.78 MeV was not considered as the matrix element of the Coriolis term producing the band mixing is sufficiently weak in this case.

We attempted a simultaneous fit to the angular distributions of the scattering from the ground state $3/2^-$ and the excited $5/2^-$ (2.43 MeV) state, a pure quadrupole state [4]. This ensured a consistent check on the multipole components of the deformed potential and the quadrupole deformation parameter during different searches to obtain an optimal fit. The same prescription was followed in both phenomenological and folding model analyses. The calculations were done using the code ECIS88 [23].

Phenomenological: In the phenomenological model the motion of the incident α particle is coupled to the intrinsic rotational motion of the quadrupole deformed ${}^9\text{Be}$ nucleus through the deformed potential

$$V(r_\alpha, \theta) = V_0(1 + e^x)^{-1} + iW_0(1 + e^{x'})^{-1} + V_C, \quad (1)$$

where $x = [(r_\alpha - R)/a]$ and $R = R_0[1 + \beta_2 Y_{20}(\theta)]$ and x' is the corresponding quantity for the imaginary part of the potential. V_C denotes the Coulomb potential. The elastic and inelastic scatterings to the members of the ground state band are generated, in the framework of symmetric rotational model, by the multipole components of the nonspherical potential $V(r_\alpha, \theta)$:

$$V_L(r_\alpha) = \int V(r_\alpha, \theta) Y_{L0}(\theta) d\Omega. \quad (2)$$

The above relation with Y_{00} gives the monopole potential for the ground state angular distribution. We used the quadrupole component $V_2(r_\alpha)$ as the inelastic form factor instead of using that of the derivative of $V(r_\alpha, \theta)$ as followed in Ref. [12]. The optical potential parameters and β 's were varied to obtain adequate fits to elastic and inelastic cross sections simultaneously. The "isoscalar" deformation parameter thus obtained was related to the electromagnestic deformation parameter through the "scaling" relation [12,24] of equating the two deformation lengths, i.e., $\beta_2 R = \beta_{2c} R_c (= \delta_2^{02})$ following the notation δ_L^{ij} , indicating the deformation length corresponding to L th multipole transition between the states denoted by i and j . The radii R and R_c are the effective "mean" radii of the nuclear potential and the charge distribution and are related to the respective root-mean-square radii [25]. The resulting charge deformation parameter β_{2c} was used to determine the intrinsic quadrupole moment Q_{20} . Assuming a prolate hard-edged shape, the quadrupole moment is expressed as [26,12]

$$Q_{20} = \frac{3Z}{\sqrt{5\pi}} R_c^2 \sigma \left[1 - \sqrt{\frac{45}{4\pi}} \sigma \right]^{-2/3},$$

$$\sigma = \beta_{2c} \left(1 + \sqrt{\frac{5}{64\pi}} \beta_{2c} \right) \left(1 + \sqrt{\frac{5}{4\pi}} \beta_{2c} \right)^{-2}, \quad (3)$$

and subsequently the reduced transition probability

$$B(E2, I_1 \rightarrow I_2) = \frac{5}{16\pi} e^2 Q_{20}^2 \langle I_1 2 K 0 | I_2 K \rangle. \quad (4)$$

Folding model: In this semimicroscopic model the interaction potentials are generated by folding an effective nucleon-nucleon interaction with the respective nuclear densities. Essential features of the model are presented in detail in Refs. [13–15]. The standard M3Y interaction [15] with a multiplicative factor to simulate the density dependence and a pseudopotential term to incorporate the single nucleon exchange was chosen to represent the effective nucleon-nucleon interaction,

$$v_{NN} = \lambda \left[7999 \frac{e^{-4r}}{4r} - 2134 \frac{e^{-2.5r}}{2.5r} \right] (1 - \gamma \rho_0^{2/3}) - 262 \delta(\mathbf{r}). \quad (5)$$

The "renormalization" factor λ was fixed from the fit to the elastic angular distribution data. The parameter γ gives a measure of the density dependence of the interaction and was chosen to be 0.4 at this energy. To construct the imaginary component of the optical potential, we assumed that the normalization factor was complex, i.e., $\lambda = \lambda_R + i\lambda_I$. The quantities (λ_R, λ_I) were varied to get a proper fit to the data.

The densities are important ingredients as the structure information is included in the model through these quantities. For the projectile α particle, we worked with a parametrized Gaussian shape for its density [15]. The densities for ${}^9\text{Be}$ were calculated from the Nilsson model

wave functions. The nucleons, in this model, move in a deformed field. We assumed a quadrupole deformed harmonic oscillator potential as the mean field where the deformation parameter was used as an adjustable quantity [27]. The nucleus ${}^9\text{Be}$ has four particles in the Nilsson orbit 1 ($\Omega = 1/2+$), four in orbit 2 ($\Omega = 1/2-$), and last odd neutron in orbit 3 ($\Omega = 3/2-$) for positive deformation. With this distribution of particles in the Nilsson orbitals, the expression for densities become

$$\rho_L^{n/p}(r_2) = [J_i][J_f]^{-1} \langle J_i L K 0 | J_f K \rangle \langle \chi_K | \hat{\rho}_L | \chi_K \rangle. \quad (6)$$

In deriving this result we used the convention of Brink and Satchler for reduced matrix elements [28]. The notation $[J]$ indicates $\sqrt{2J+1}$. $\hat{\rho}_L$ is the L th component of the density operator. The intrinsic wave function χ_K is of determinantal form with Nilsson single particle wave function χ_{Ω_i} , Ω_i are the projections of single particle j_i 's on the symmetry axis, and $K = \sum_i \Omega_i$. Expanding χ_{Ω_i} in the harmonic oscillator basis, the intrinsic matrix element can be written as

$$\langle \chi_K | \hat{\rho}_L | \chi_K \rangle_{p/n} = \sum_i \left[\sum_{N\Lambda} \sum_{N'\Lambda'} a_{N\Lambda}^i a_{N'\Lambda'}^i u_{N\Lambda}(r_i) u_{N'\Lambda'}(r_i) \right. \\ \left. \times \langle l' \Lambda | Y_{L0} | l \Lambda \rangle \right]. \quad (7)$$

i denotes summation over all occupied proton and neutron orbitals, respectively. $u_{N\Lambda}(r_i)$ are the radial wave functions of the harmonic oscillator basis states. We used an oscillator parameter $b_0 = 1.664$ fm as used in the shell model calculation for ${}^9\text{Be}$ [4]. The a coefficients were determined by diagonalizing the Hamiltonian with only quadrupole deformation using the code RPMAIN [29]. The calculation also included the N and $N \pm 2$ mixing of the major oscillator shells and used the values of the parameters for the spin-orbit and high-spin correction terms (κ, μ) from Ref. [2]. The intrinsic single particle quadrupole moment was determined from χ_{Ω_i} 's as

$$Q_0^{(i)} = 2 \sqrt{\frac{4\pi}{5}} \int \chi_{\Omega_i} r_i^2 Y_{20}(\hat{r}_i) \chi_{\Omega_i} d\mathbf{r}_i \quad (8)$$

and $Q_0 = \sum_i Q_0^{(i)}$. With the densities from Eq. (6), the transition multipole matrix elements for protons and neutrons were evaluated from the relation

$$M_L^j = \int \rho_L^j(r_2) r_2^{L+2} dr_2 \quad (j=p, n) \quad (9)$$

and hence the "isoscalar" transition matrix $M_L(IS) = M_L^p + M_L^n$. The reduced transition probability is given by

$$B(E2, I_1 \rightarrow I_2) = \frac{(2I_2 + 1)}{(2I_1 + 1)} |M_2^p|^2. \quad (10)$$

TABLE I. Optical potential parameters.

OM	V_0 (MeV)	r_0 (fm)	a_0 (fm)	W_0 (MeV)	r_1 (fm)	a_1 (fm)	$J_V/4A$ (MeV fm ³)	$J_W/4A$ (MeV fm ³)	r_{rms} (fm)
Set 1	174.2	1.491	0.587	17.55	1.491	0.587	-858.80	-86.52	3.36(Re) 3.36(Im)
$\beta_{2r} = \beta_{2i} = 0.52$									
Set 2	145.31	1.446	0.597	69.60	0.932	0.597	-666.35	-120.00	3.31(Re) 2.74(Im)
$\beta_{2r} = 0.573, \beta_{2i} = 0.604$									

IV. RESULTS AND DISCUSSION

Phenomenological: As described earlier, a deformed potential was used in the coupled channel formalism to generate the $3/2^-$ and $5/2^-$ angular distributions. We started our

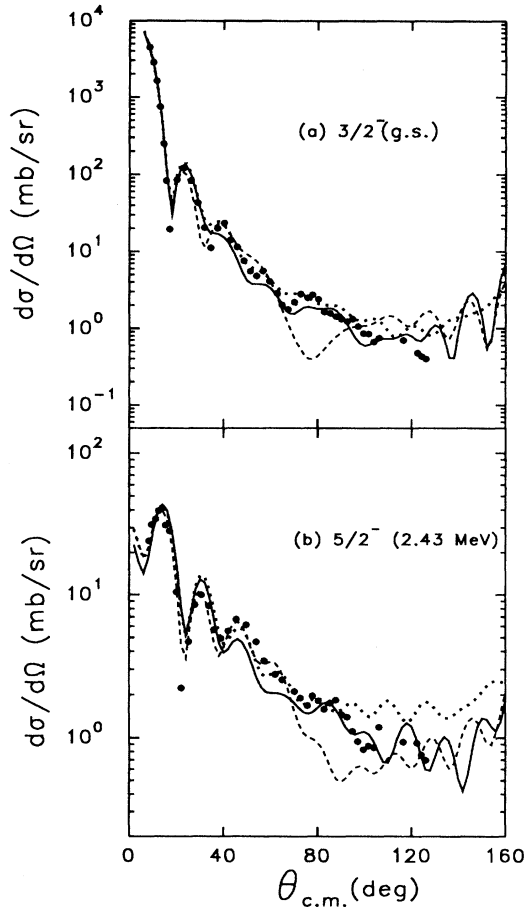


FIG. 2. Fits to the angular distributions of (a) elastic and (b) inelastic scattering of $\alpha + {}^9\text{Be}$ at 65 MeV. The dotted curve represents a phenomenological CC calculation where only $5/2^-$ is coupled to the $3/2^-$ ground state with potential set 2. The dashed curve represents the same calculation with potential set 1. The solid curve in the figures indicates the CC calculation for $3/2^- \leftrightarrow 5/2^- \leftrightarrow 7/2^-$ coupling with potential set 2.

analysis with the optical model (OM) parameters of Ref. [11] (set A65', Table I). Angular distributions obtained with these parameters are shown in Fig. 2 (dashed curve). The parameters are given as set 1 in Table I of this presentation. With $3/2^- \leftrightarrow 5/2^-$ coupling including the self-couplings and Coulomb excitation, the potential reproduced the data quite well in the forward angles. However, in the angular region beyond $\theta_{\text{c.m.}} = 60^\circ$ the calculated distributions, with prominent dips around 80° , failed to describe the qualitative nature of the data. A possible reaction channel, indistinguishable from the elastic experimentally, that can have appreciable contribution at large angles is the heavy particle pickup (HPPU). In the case of α scattering from ${}^9\text{Be}$, we calculated the contribution of the reaction channel ${}^9\text{Be}(\alpha, {}^9\text{Be})\alpha$ and found that it enhances the angular distribution beyond $\theta_{\text{c.m.}} \approx 140^\circ$. As our data extends only up to $\theta_{\text{c.m.}} \approx 126^\circ$ we persisted with the potential scattering description of the large angle data. We varied the potential parameters with more emphasis on the geometry of the absorptive part. A detailed χ^2 search, with the same $3/2^- \leftrightarrow 5/2^-$ coupling and corresponding self-coupling terms, allowing for some variations in the real and imaginary depths, resulted in a set of parameters given as set 2 in Table I. Corresponding angular distributions are shown in Fig. 2 (dotted curves). A comparison of deformed potentials is shown in Fig. 3. An optical potential, like set 2, with "surface transparent" (i.e., $r_i > r_0$) behavior is not unlikely in the case of α scattering from ${}^9\text{Be}$ as shown by Hauser *et al.* [30]. Though this behavior is more common to higher bombarding energies where refractive scattering dominates at large angles, what we observe is that, even at 65 MeV, to describe the large angle data for ${}^9\text{Be}$ the potential needs to possess some amount of transparency at the surface. With the same set of parameters if the $7/2^-$ state is included in the coupling scheme (with only $L=2$ coupling) the fit to the elastic data improves considerably (solid lines) over the whole angular range. On the other hand, the fit to the $5/2^-$ (2.43 MeV) state angular distribution, though it becomes worse in the angular range $35^\circ < \theta_{\text{c.m.}} < 70^\circ$, shows a much better agreement in the range beyond $\theta_{\text{c.m.}} = 70^\circ$.

In Fig. 4, the effect of "reorientation" contributions on the cross section data have been shown explicitly. The solid curves in the figures represent the angular distributions with the $3/2^- \leftrightarrow 5/2^- \leftrightarrow 7/2^-$ coupling and the respective reorientation terms. When the ground state reorientation coupling ($3/2^- \leftrightarrow 3/2^-$, $L=2$) was switched off the same potential pa-

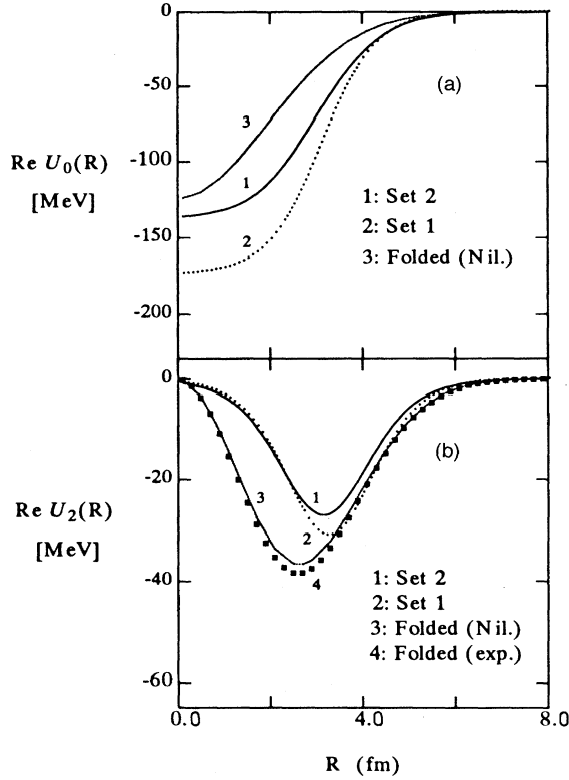


FIG. 3. Real parts of the (a) monopole and (b) quadrupole potentials. The quadrupole potential shown here corresponds to $3/2^- \rightarrow 5/2^-$ transition. In (b) the curve shown in black boxes (4) is the quadrupole potential generated by model-independent transition densities obtained from electron and proton scattering data.

parameters yielded angular distributions given by the short dashed curves in the figures. The dotted curves in the figures show the angular distributions without any reorientation couplings. From Figs. 4(a) and 4(b) it is obvious that the ground state quadrupole reorientation coupling has significantly greater influence than the excited state reorientations on the angular distributions.

The deformation lengths and the corresponding β deformations are tabulated in Table II. It is to be noted that in the definition of deformation length (δ_2^{02}) we used the mean radii of the deformed distributions following Ref. [1]. In the last two columns of Table II the calculated and experimental intrinsic quadrupole moments are shown. The present CC calculation with potential set 2 yielded a quadrupole deformation length $\delta_2^{02} = 2.448$ fm for the $3/2^- \rightarrow 5/2^-$ transition. This value is somewhat greater than the value of 1.97 fm obtained by Cook and Kemper [31] but matches well with the value 2.5 fm considering the observed energy dependence of deformation length in the study of ${}^6\text{Li}$ scattering from ${}^9\text{Be}$ by Muskat *et al.* [32]. Subsequently the charge deformation parameter β_{2c} is found to be 0.755 ± 0.11 using the charge rms radius value of 2.51 fm [33]. The δ_2^{02} obtained with potential set 1 is also within 10% of this value and the resulting charge deformation also lies within the error bar of the value of 0.755. The calculated intrinsic quadrupole mo-

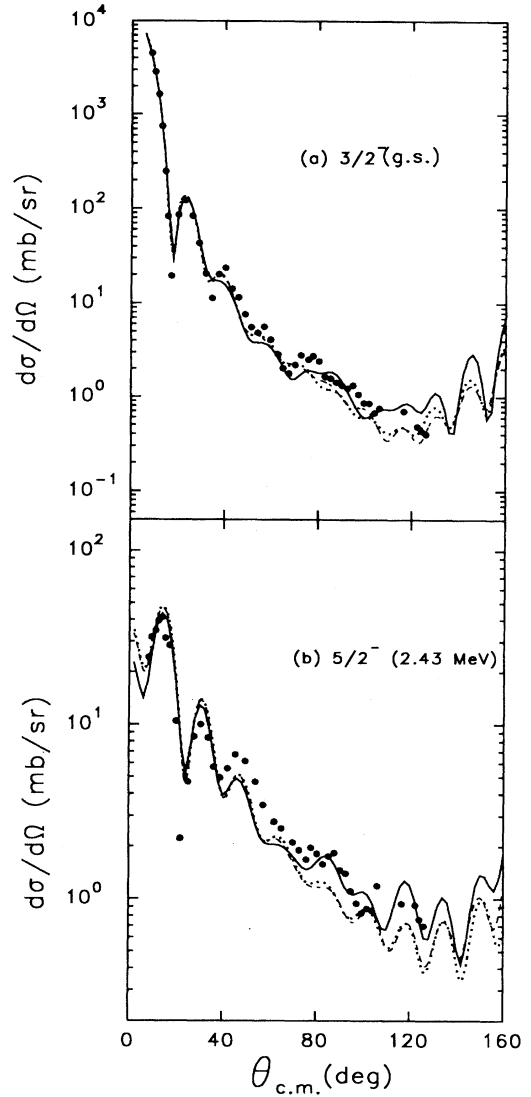


FIG. 4. Fits show the effect of reorientation coupling in the angular distributions of (a) elastic and (b) inelastic scattering of $\alpha + {}^9\text{Be}$ at 65 MeV. The solid curve represents the phenomenological CC calculation including the three channels and with potential set 2 as in Fig. 3. The dashed curve represents the same calculation without the ground state reorientation only while the dotted curve describes the angular distribution with no reorientation coupling.

ment of $29.68 e \text{ fm}^2$ compares well with the experimental value of $29.30 e \text{ fm}^2$ [4].

Folding Model: The monopole and quadrupole components of the folded potential used in the CC calculation are constructed from the Nilsson model wave functions. In Figs. 3(a) and 3(b) the curves marked 3 represent the two components of the potential. The coefficients $a_{N\lambda}$ generating the intrinsic wave function in the harmonic oscillator basis to calculate the density components are given in Table III. The parameters μ and κ of the Nilsson Hamiltonian are shown in the table. We worked with a quadrupole deformation $\delta_2 =$

TABLE II. Deformation parameters.

OM	β_2	R^a (fm)	δ_2^{02} (fm)	R_c (fm)	β_{2c}	Q_{20} ($e \text{ fm}^2$)	$Q_{20}(\text{expt})^b$ ($e \text{ fm}^2$)
Set 1	0.52	4.32	2.246	3.24	0.69	26.64	29.30
Set 2	0.573	4.27			0.755	29.684	

^a $R = \sqrt{5/3} \langle r^2 \rangle^{1/2}$ [11].

^bReference [4], Table V.

0.564 and oscillator parameter $b_0 = 1.664$ fm that yielded a proton distribution showing reasonably good agreement with the electron scattering form factor data [4] except at large momentum transfer values. For the neutron densities, however, we used the same deformation and b_0 . This is not a particularly good approximation as it assumes that the neutrons are equally tightly bound in ${}^9\text{Be}$ as the protons, though the chosen value of δ_2 is close to the deformation which gives the minimum energy configuration for the neutrons in ${}^9\text{Be}$. In spite of this limitation, the model predicted reasonably good shape for the components of the mass density. In Fig. 5 we have compared the proton and neutron quadrupole densities with those obtained from electron and proton inelastic scattering experiments [4,9]. The resulting transition potentials are shown in Fig. 3(b). Clearly the model-dependent transition potential is not much different from the

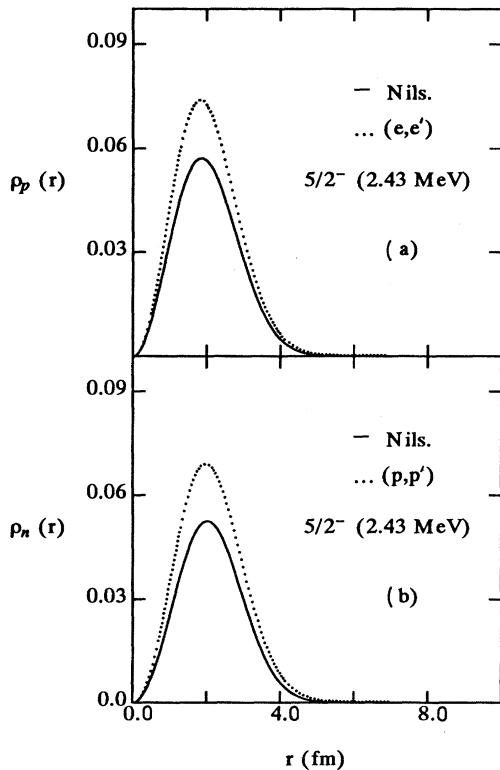


FIG. 5. The quadrupole transition densities for $3/2^- \rightarrow 5/2^-$ transition from Nilsson model calculation (solid lines). Experimental proton density in (a) and neutron density in (b) are from Ref. [4] and Ref. [9], respectively.

TABLE III. Coefficients of harmonic-oscillator (HO) basis states for Nilsson wave functions ($\eta=8.0$, $\delta_2=0.564$, $\mu=0.0$, $\kappa=0.08$).

$\Omega = 1/2^+$		$\Omega = 1/2^-$		$\Omega = 3/2^-$	
$\epsilon = 1.662$		2.203		2.872	
$N\Lambda\Sigma$	$a_{N\Lambda}$	$N\Lambda\Sigma$	$a_{N\Lambda}$	$N\Lambda\Sigma$	$a_{N\Lambda}$
220+	0.20645	330+	0.25096	331+	0.22475
200+	0.05305	310+	0.19288	311+	-0.00645
221-	0.01826	331-	0.04957	332-	0.02379
000+	0.97685	311-	0.00861	111+	0.97411
		110+	0.93755		
		111-	0.13522		

model-independent one and for the latter calculation we used, consistently, the model-dependent transition potential. In Table IV the relevant quantities obtained from Nilsson model calculation are compared with the shell model calculations and the experimentally measured values. The transition matrices, from the model calculation, are multiplied with effective charges suitable for p -shell nuclei [4,34]. The δ deformation value used in the calculation yields a spectroscopic quadrupole moment which is much less than the experimental value. A possible increment in the deformation affects the rms radius of the distribution that is otherwise very well reproduced. A deformation $\delta_2 = 0.564$ corresponds to $\beta_2 = 0.66$ [35].

As in the phenomenological case, quadrupole form factors for the self-coupling terms are of same shape as the transition potential differing only in magnitude through the geometrical factors. The angular distributions for the $3/2^-$ and $5/2^-$ states predicted by the folded potentials with the same set of couplings are given in Figs. 6(a) and 6(b). The renormalization factors necessary to fit the data are found to be $\lambda_R = 1.0$ and $\lambda_I = 0.25$. For the potentials folded with densities from experiments, the factors are $\lambda_R = 0.98$ and $\lambda_I = 0.26$. We note that in both the cases the values of λ_R are close to unity unlike the scattering of ${}^9\text{Be}$ as projectile from different heavier mass targets [15,16]. As in the case of ${}^3,4\text{He}$ scattering from ${}^6\text{Li}$ at several energies [17], any large reduction of strength is not required in this case also. This is true for the folding with model-independent densities from experiment as well.

With the folded monopole and quadrupole components of the optical potential, the CC calculation predicted an elastic angular distribution which is rather flat in nature beyond

TABLE IV. The matrix elements.

	Nilsson model	Shell model ^a	Experiment ^{a,b}
Q ($e \text{ fm}^2$)	4.33	4.31	5.86
M_p ($e \text{ fm}^2$)	4.706	4.61	5.54
r_p (fm)	3.267		3.27
M_n ($e \text{ fm}^2$)	4.658	4.42	6.48
r_n (fm)	3.31		3.68
M_n/M_p	0.99	0.96	1.17
$M(\text{IS})$ ($e \text{ fm}^2$)	9.364	9.03	12.02
$B(E2) \uparrow$ ($e^2 \text{ fm}^4$)	33.27	32.2	46.0

^aReference [4].

^bReference [9].

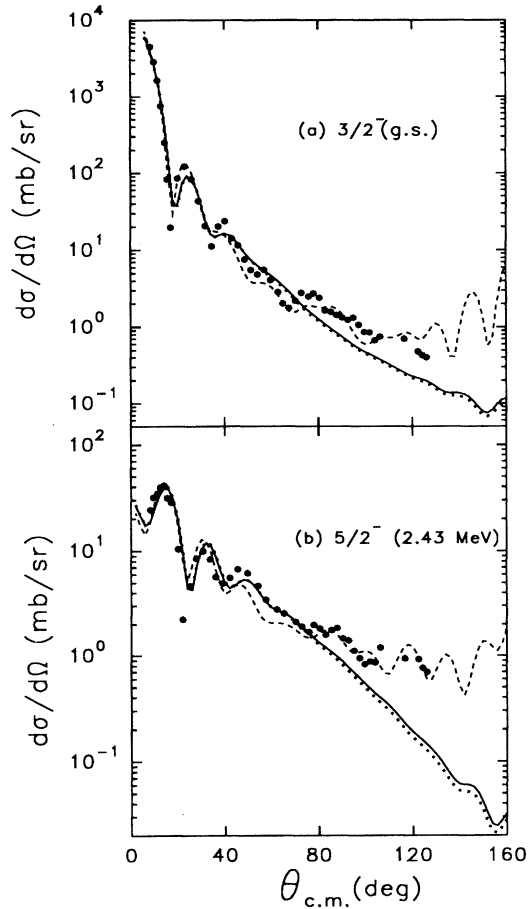


FIG. 6. Angular distributions of (a) elastic and (b) inelastic with folded potentials in the CC calculation employing the three channel coupling and including the respective reorientation terms. The solid curves are with the densities from Nilsson model calculation and the dotted curves are with model independent densities determined from electron and proton scattering experiments (Refs. [4,9]). The dashed curves in the figures correspond to phenomenological potential set 2 for comparison. Solid spheres represent the experimental data.

$\theta_{c.m.} \approx 40^\circ$. A possible reason for this deficiency in the fit to the elastic data is the falloff of the $L=0$ component of the potential in the most sensitive radial region for the strongly absorbing projectile alpha [see Fig. 3(a)]. The limitation is in the proper determination of the neutron distribution of ${}^9\text{Be}$. The loosely bound nature of the odd neutron should introduce a larger radial extent in the mass distribution as well as in the folded potential. Unlike the $3/2^-$ state, a reasonably good fit is obtained for the angular distribution of the scattering from $5/2^-$ excited state. The predicted distribution reproduced the data relatively better than the phenomenological calculation upto $\theta_{c.m.} \approx 75^\circ$. With a sharp fall beyond $\theta_{c.m.} \approx 80^\circ$, it underestimates the large angle data. However, the qualitative nature of the fits indicates that the angular distributions of the $3/2^-$ and $5/2^-$ states do not allow a larger value of β_2 in the Nilsson model calculation and a value of

0.66 is within the range of values obtained from phenomenological calculation.

V. SUMMARY

The elastic and inelastic scatterings of 65 MeV α particles from ${}^9\text{Be}$ have been studied. The measured cross sections of $3/2^-$ and $5/2^-$ states extending over a wider angular range are analyzed in the coupled channel framework in symmetric rotor model. The first three members of the ground state band are coupled with proper spins including the self-coupling (reorientation) contributions.

In the phenomenological analysis we attempted to ascertain the β_2 deformation of ${}^9\text{Be}$. We performed the calculations with two different sets of potentials. An attempt to fit the large angle data leads to the second set (set 2) of potential parameters. However, the rms radii of these shapes do not differ by more than 5%. Taking the radius of the equivalent spherical distribution proportional to the rms radius of the deformed shape the β_{2c} value from our best fit parameter set is 0.755 ± 0.11 . This value is still quite low compared to the results of the electromagnetic probes which predict a value around 1.1.

It is observed that while the coupling to $7/2^-$ state improves the fit to the $3/2^-$ state angular distribution considerably, the prediction for $5/2^-$ state becomes worse. Ground state reorientation has a much more dominating effect than the excited state reorientations in predicting the angular distributions for both the states. With proper spins of the states the reorientation coupling simulates the quadrupole scattering effect in the elastic angular distribution quite well.

We also analyzed the data with folded potentials in the same coupling scheme. In a way this has put a more stringent constraint on the shape of the potentials. The densities were constructed from Nilsson model calculations for ${}^9\text{Be}$ using the deformation as a parameter. The different structure observables from the calculation compare well with the shell model calculation but to some extent are smaller than the experimental values. The model yielded a β_2 deformation value of 0.66. This value is close to the deformations corresponding to the minimum energy configurations of protons and neutrons in the Nilsson model description of ${}^9\text{Be}$ and it lies within the limit of the phenomenologically obtained value. The agreement of the resulting angular distributions with the data indicates that, as in the case of scattering of lighter projectiles from ${}^6\text{Li}$, the model can be used to describe α scattering from loosely bound ${}^9\text{Be}$ to a good extent and also it can be employed in the description of different transfer reactions involving α and ${}^9\text{Be}$.

ACKNOWLEDGMENTS

The authors would like to thank Prof. S. Sen and Prof. S. Bhattacharya for helpful discussions and valuable suggestions. One of us (H.M.) is grateful to Prof. J. Raynal of Service de Physique Theorique, Saclay, France for his constructive suggestions and comments. The help and cooperation received from the members of the VECC Control Room and Target Laboratory are gratefully acknowledged.

- [1] A. Bohr and B.R. Mottelson, *Nuclear Structure* (Benjamin, New York, 1975), Vol. 2, p. 136.
- [2] D. Vinciguerra and T. Stovall, Nucl. Phys. **A132**, 410 (1969).
- [3] A.G. Slight, T.E. Drake, and G.E. Bishop, Nucl. Phys. **A208**, 157 (1973).
- [4] J.P. Glickman *et al.*, Phys. Rev. C **43**, 1740 (1991).
- [5] D.F. Geesaman *et al.*, Phys. Rev. C **18**, 2223 (1978).
- [6] H.J. Vatova, T.B. Clegg, E.J. Ludwig, and W.J. Thompson, Nucl. Phys. **A204**, 529 (1973).
- [7] G. Roy *et al.*, Nucl. Phys. **A442**, 686 (1985).
- [8] J.J. Kelly *et al.*, Phys. Rev. C **38**, 1490 (1988).
- [9] S. Dixit *et al.*, Phys. Rev. C **43**, 1758 (1991).
- [10] R.G. Summer-Gil, Phys. Rev. **109**, 1591 (1958).
- [11] M.N. Harakeh, J. Van Popta, A. Saha, and R. Siemsen, Nucl. Phys. **A344**, 15 (1980).
- [12] R.J. Peterson, Nucl. Phys. **A377**, 41 (1982).
- [13] A.M. Kobos *et al.*, Nucl. Phys. **A384**, 65 (1982); A.M. Kobos, B.A. Brown, R. Lindsay, and G.R. Satchler, *ibid.* **A425**, 205 (1984).
- [14] Subinit Roy *et al.*, Phys. Rev. C **45**, 2904 (1992).
- [15] G.R. Satchler and W.G. Love, Phys. Rep. **55**, 183 (1979).
- [16] G.R. Satchler, Phys. Lett. **83B**, 284 (1979).
- [17] T. Sinha, Subinit Roy, and C. Samanta, Phys. Rev. C **47**, 2994 (1993); **48**, 785 (1993).
- [18] F. Ajenberg-Selove, Nucl. Phys. **A490**, 1 (1988).
- [19] G.R. Satchler, Nucl. Phys. **A100**, 467 (1967).
- [20] S. Tanaka *et al.*, J. Phys. Soc. Jpn. **45**, 733 (1978).
- [21] S. Cohen and D. Kurath, Nucl. Phys. **73**, 1 (1965).
- [22] P.D. Kunz, Ann. Phys. (N.Y.) **11**, 275 (1960).
- [23] J. Raynal, computer code ECIS88 (unpublished).
- [24] A.M. Bernstein, Annu. Rev. Nucl. Sci. **3**, 325 (1969).
- [25] W.D. Meyers, Nucl. Phys. **A204**, 465 (1973).
- [26] M.A. Preston, *Physics of the Nucleus* (Addison-Wesley, Reading, MA, 1972).
- [27] S.G. Nilsson, Mat. Fys. Medd. Dan. Vid. Selsk. **29** (1966).
- [28] D.M. Brink and G.R. Satchler, *Angular Momentum* (Oxford University Press, Oxford, 1971).
- [29] S. Bhattacharya, computer code RPMAIN (unpublished).
- [30] G. Hauser *et al.*, Nucl. Phys. **A128**, 81 (1969).
- [31] J. Cook and K.W. Kemper, Phys. Rev. C **31**, 1745 (1985).
- [32] E. Muskat, J. Carter, R.W. Fearick, and V. Hnizdo, Nucl. Phys. **A581**, 42 (1995).
- [33] I. Tanihata *et al.*, Phys. Rev. Lett. **55**, 2676 (1985).
- [34] D.J. Millener *et al.*, Phys. Rev. C **39**, 14 (1989).
- [35] R. Bengtsson *et al.*, Phys. Scr. **39**, 196 (1989).